

Electromagnetic Characteristic Analysis and Optimization Design of a Novel HTS Coreless Induction Motor for High Speed Operation

Bin Liu, Rod Badcock, Hang Shu, Lu Tan, Jin Fang

Abstract—We develop a novel high temperature superconducting (HTS) induction motor with saddle-shaped HTS armature windings, which adopts the structure with a coreless stator and a conventional squirrel-cage rotor, that is aimed to lightweight and higher speed. In this paper, the saddle-shaped HTS armature windings is composed of three layers of coils, of which each layer is arranged in six along circumferential direction. Moreover, the detailed production method of the coil is illustrated. According to the electromagnetic field theory, the electromagnetic characteristic of the newly designed HTS coreless induction motor are investigated including the flux density distribution and the torque ripple under the condition of no-load and rated load. Then based on the initial geometry model, the arrangement structure of the HTS coils is optimized and analyzed. By optimizing the rotation angle of the HTS coil layer along the circumferential direction, it is found that the magnetic field perpendicular to the tape surface in the optimized shape coils significantly decreases compared with that in the initial shape coils. In addition, it is also noticed that not only the torque ripple becomes smaller, but also the distortion of the air-gap magnetic flux density is improved. Finally, a satisfactory coils arrangement structure model is obtained, which is intended to be utilized for HTS coreless motor.

Index Terms—HTS, Coreless induction motor, saddle-shaped coils, torque ripple.

I. INTRODUCTION

DU E to the advantages of light weight, high specific power and high efficiency, the high temperature superconducting coreless motor has become a hot research topic in recent years. Research shows that the magnetic field of HTS motor generated by HTS material can be higher compared with that of the conventional motor, so that the iron core can be considerably reduced, even eliminated [1-3].

The majority of HTS coreless motor adopts a form of the fully superconducting structure without iron core in stator and rotor, in which the armature winding is composed of superconducting coils and the rotor adopts superconducting coils or superconducting bulks[4]-[11]. In these literatures, although the removal of stator and rotor core with the use of

fully HTS materials are more conducive to the development of superconducting motor, the HTS tape subjected to bending stress or tensile stress will lead to its critical current decline. In particular, fully superconducting motors will consume a lot of superconducting materials and increase the complexity of the rotor cooling system. Most importantly, the rotor is limited to a high-speed operation owing to the rotor dynamic seal problem [12]. Therefore, in order to avoid the influence of superconducting materials and improve the mechanical strength of the rotor, we have designed the HTS coreless induction motor(CIM), in which rotor part adopts conventional design and the static stator core is removed. This design is conducive to the development of high-power high-speed HTS coreless motor.

II. ELECTROMAGNETIC THEORY DESIGN OF HTS CIM

According to the theory of motor design, the output power of the motor is related to its contour size and electromagnetic parameters as follows[13]:

$$D^2 l = \frac{6.1 K_B}{a'_p K_{NM} K_{dp} A B_\delta \eta \cos \varphi n} \frac{P}{n} \quad (1)$$

where, D is the armature diameter, l is the armature valid length, K_B is the ratio of induction voltage at rated condition, P is the output power, a'_p is the polar arc coefficient, K_{NM} is air-gap field waveform coefficient, K_{dp} is the winding coefficient, A is the electric load, B_δ is the air-gap magnetic density maximum, η is the efficiency, $\cos \varphi$ is the power factor, n is the motor speed.

The electric load A can be computed as:

$$A = \frac{2m I_m W_m}{\pi D} \quad (2)$$

where, m is the phase number, I_m is the current effective value of armature winding, W_m is the series turns per phase of armature winding.

By (1) and (2), an approximate expression of the output power of a motor can be obtained:

$$P \propto n D l W_m I_m \quad (3)$$

As can be seen from (3), the greater the armature current of

This work was supported by the Fundamental Research Funds for the Central Universities(E17JB00280) and grants from the National Key Laboratory on Aero-Engines (No.9140C410405150C41005), China.

B. Liu, H. Shu, L. Tan and J. Fang are with School of Electrical Engineering, Beijing Jiaotong University, Beijing, China (e-mail: 14117396@bjtu.edu.cn; 16121513@bjtu.edu.cn; 16126047@bjtu.edu.cn; jfang@bjtu.edu.cn;).

R. Badcock is with Robinson Research Institute, Victoria University of Wellington, New Zealand (e-mail: Rod.Badcock@vuw.ac.nz).

the motor and the higher the rotor speed, the easier it is to obtain a larger output power under the smaller volume. So in order to further reduce the volume of superconducting motor, improve the power density, and obtain higher speed, only superconducting motors with HTS armature are the inevitable direction of future high-speed superconducting motor.

III. BASIC DESIGN AND ANALYSIS MODEL

A. Armature winding design and structure

The design of armature winding is the key technology of HTS coreless motor. The critical current of HTS coil is mainly influenced by the magnetic field perpendicular to the tape surface and the bending radius of tape. The motor winding adopts the Japanese Fujikura GdBCO tape. GdBCO tape performance parameters are shown in Table I. Based on the data provided by the Fujikura superconductor company, the critical current curves of GdBCO at 77K in parallel and perpendicular fields respectively are obtained, as shown in Fig. 1.

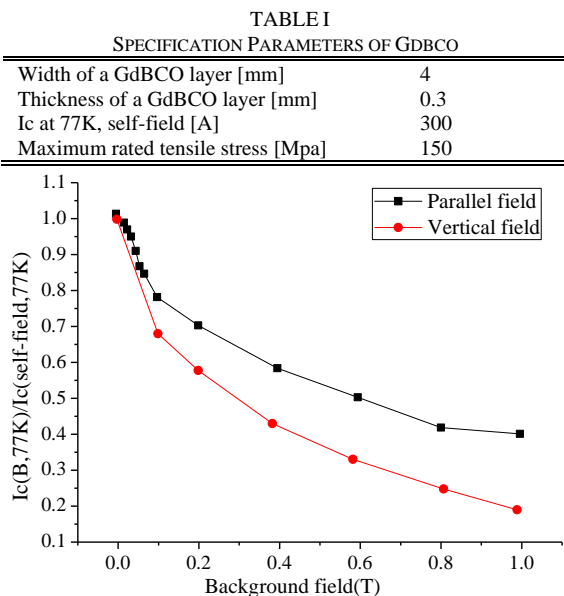


Fig. 1. Critical current change curve of GdBCO tape in background field

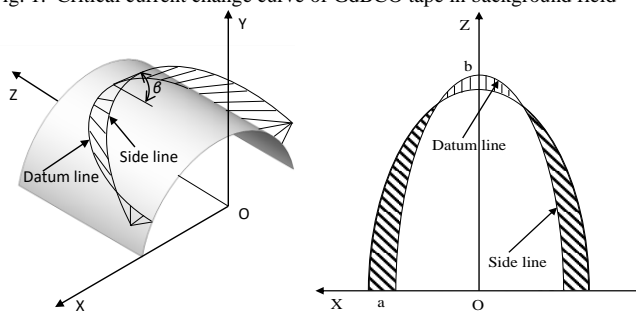


Fig. 2. Schematic diagram of one end of saddle-shaped coil

The study shows that the critical current of GdBCO tape decreases by less than 3% when the GdBCO torsion angle is not more than 36.48 deg/cm. But when the torsion angle increases to 60.8 deg/cm, the critical current decreases by 30%. The rated current of the motor designed is 195A with two parallel branches, so the critical current surplus of superconducting tape is very large. In the design process of the saddle coil, the torsion

angle of the end is strictly controlled, and it is the manufacturing difficult point.



Fig. 3. 3D model of armature coil

When the saddle-shaped coil is wound, it is necessary to design the reference line for coil on the semi-circular plate, and set the angle between the tape and the semi-circular plate. The results show that in order to minimize the bending of the superconducting tape at the end, the high quality saddle-shaped coil wound is required to control the angle β between the inner ring tape in the coil and the semi-circular plate, which is generally 45°. The schematic design of one end of the saddle-shaped coil is shown in Fig. 2, wherein a, b are the length of semi major axis and minor axis of the ellipse respectively. Fig. 3 shows the 3D structure of the saddle-shaped coil.

B. Electromagnetic FEM Analysis of Basic Model

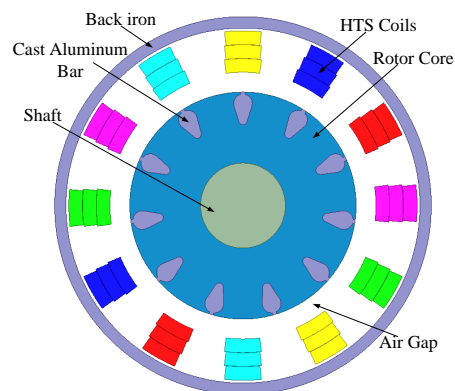


Fig. 4. Basic structure model of HTS CIM

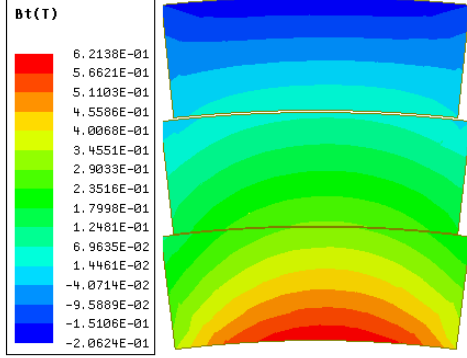
A basic structure model of HTS CIM is shown in Fig. 4. The motor is mainly composed of saddle-shaped HTS armature coils, a squirrel cage rotor and ferromagnetic shield. It can be observed that the motor adopts the air-core structure in stator and centralized winding arrangement. Each phase windings consist of three-layer saddle-shaped HTS coils. Each layer arranges six coils in the circumferential direction, and the whole stator part is cooled by liquid nitrogen to 77K.

Different from the conventional coreless machine which uses permanent magnet rotor or HTS rotor to offer high speed, the HTS CIM can provide much higher ampere-turns for the armature windings to significantly increase the machine power density. Table II is the primary design parameters of the motor.

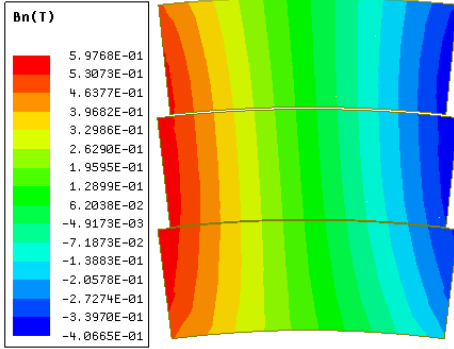
TABLE II
PRELIMINARY DESIGN PARAMETERS OF HTS CIM

Rated output power [kW]	18
Rated current [A]	195
Rated frequency [Hz]	100
Synchronous speed [r/min]	6000

Number of poles	2
Number of parallel branches	2
Rotor outer diameter [mm]	80
Rotor inner diameter [mm]	30
Number of rotor slots	11
Saddle-shaped coil turns	50
Coil inner diameter [mm]	12
Coil outer diameter [mm]	27
Electromagnetic air gap [mm]	7
Back iron thickness [mm]	10



(a) Vertical direction of HTS coils



(b) Horizontal direction of HTS coils

Fig. 5. Flux density distribution of three-layer HTS coils on **basic** model

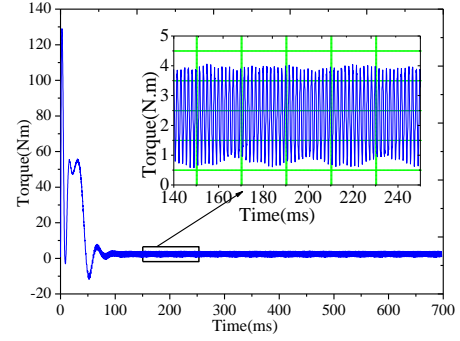
To verify the validity of the HTS CIM, the performances are analyzed based on the 2D finite-element model in Fig.4. When the HTS coils enter the current of 195A, the flux density distribution in the tangential and normal directions of the three-layer superconducting coils is predicted, and is given in Fig.5. The tangential and normal directions are the vertical and horizontal directions of the superconducting coils subjected to the magnetic field. Fig. 5 shows the results the maximum flux density at vertical direction is 0.621T, and that is 0.597T at the horizontal direction. The flux density operating perpendicular to the face of GdBCO tape dictates the current of HTS coils. According to Fig.1, the critical current is not exceeded at 77 K and the HTS coils can be operated continually. However, the performance of superconducting materials is still not fully developed, but also need to further optimize the structure of the coils.

The torque ripple rate of the motor in stable operation is defined as the following formula:

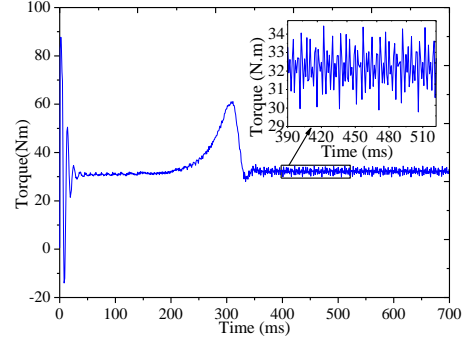
$$k = (T_{\max} - T_{\min}) / T_{av} \quad (4)$$

where, T_{\max} is the maximum torque, T_{\min} is the minimum torque,

T_{av} is the average torque.



(a) with no-load



(b) with load

Fig. 6. Transient curve of torque on basic model

According to Fig. 6 (a), when the motor reaches a steady state with no-load, the maximum torque is 4.06 Nm, the minimum torque is 0.58 Nm, the average torque is 2.36 Nm, and the motor torque ripple rate is 147.5%. The torque curve of the motor is shown in Fig. 6 (b) when the motor is applied to 30 Nm. As can be seen from the figure, when the motor reaches a steady state, the maximum torque is 34.44 Nm, the minimum torque is 29.69 Nm, the average torque is 32.34Nm, and the motor torque ripple rate is 14.9%.

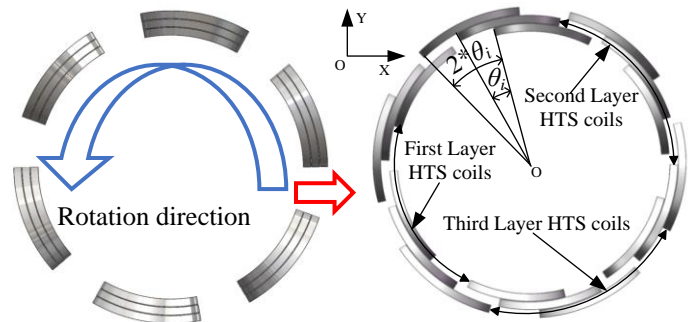


Fig. 7. Optimized windings arrangement structure model

IV. OPTIMIZATION DESIGN AND FINALIZED MODEL

Although the removal of the stator core eliminates the influence of cogging torque, it has also led to the increase of the main magnetic circuit reluctance and leakage flux, which weakens the air-gap magnetic field. In order to reduce the magnetic resistance and leakage flux and increase the air-gap magnetic field, the arrangement of the HTS coils is changed to fill the vacancy left behind the removal of iron core. To do this,

the three-layer superconducting coils are rotated around the z-axis. The first layer of the coils remains motionless, and in the same direction of rotation, the rotation angle of the second layer coils is half of the rotation angle of the third layer coils. The final rotation structure is shown in Fig. 7.

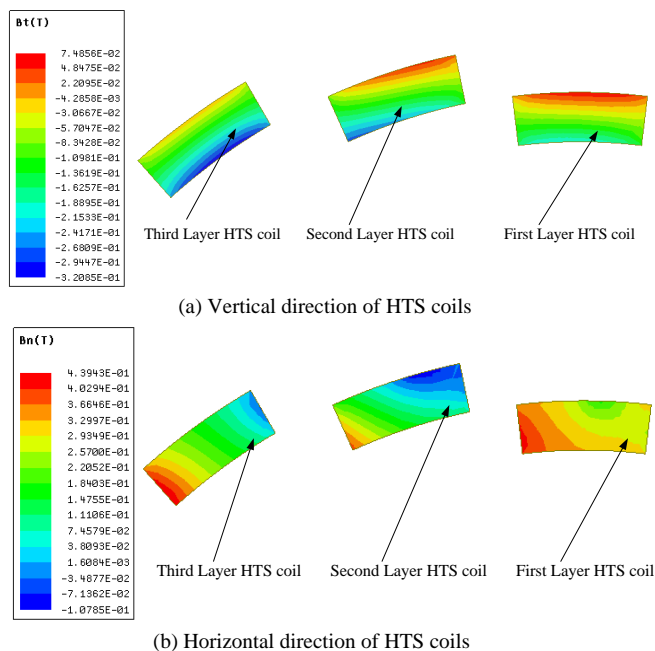


Fig. 8 Flux density distribution of the optimized three-layer HTS coils

In order to optimize the structure of the HTS windings, the flux density perpendicular to the tape surface is chosen as the objective function, which is the function of rotation angle, θ_i ($i=1, 2, 3, \dots$). The constraint condition is that T_{torq} keeps constant, where T_{torq} is the rated torque of HTS CIM. B_n and B_t are the flux density in the horizontal and the vertical directions of the HTS coils.

The optimization design problem of HTS windings can be drawn as follows:

Minimize

$$B_n = f(\theta_i), \quad i=1,2,\dots \quad (7)$$

subject to

$$T_{torq} = constant \quad (8)$$

After the calculation and comparison, the performance of the motor is best when the second layer rotates θ_i to 18° and the third layer rotates to 36° .

Fig. 8 is the distribution of flux density in the vertical direction and horizontal direction of the optimized superconducting three-layer coils. It can be seen from the graph that the vertical magnetic field and horizontal field are greatly reduced when the superconducting coils rotate a certain angle. The maximum vertical flux density is 0.321T and the maximum horizontal flux density is 0.439T, which is decreased by 48.3% and 26.5% respectively than the basic coils structure.

Fig. 9 shows the optimized transient torque curve of the HTS CIM with no-load, in which the torques ripple decrease drastically. The maximum torque of the optimized structure is 2.87Nm in the stable operation and the minimum torque is

1.65Nm. The torque ripple rate of the optimized structure is only 51.4%, which is decreased by approximately 65.2% compared with the basic structure.

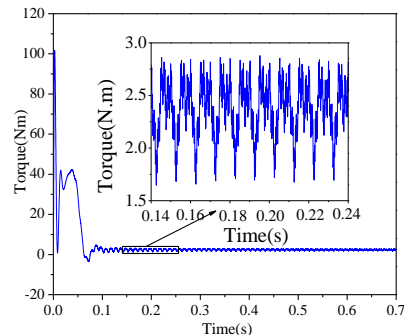


Fig. 9 Optimized transient curve of torque

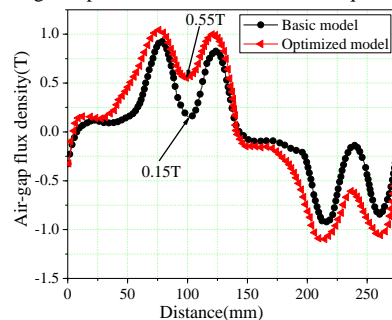


Fig.10 Distribution of the air-gap density

Fig.10 shows air-gap flux density distributions for the basic model and the optimized model. Both of them are approximate to the saddle waveforms. The optimized model shows slightly higher waveform amplitude as compared with the basic one. Moreover, there exists remarkable phase shifting between two waveforms because of the change of HTS coils arrangement structure. The flux density is increased from 0.15T to 0.55T at the lowest point of the saddle-shaped waveform, and to some extent, the distortion of the air-gap magnetic field caused due to the absence of iron core is improved.

V. CONCLUSION

In this paper, a novel HTS CIM was studied based on the minimization of the torque ripple and the perpendicular magnetic field component to the tape surface. The results shows that the performance of HTS materials is still not fully developed, but also needs further optimization. Based on the initial structure, the arrangement optimization design of the superconducting windings was carried out. The three-layer superconducting coils are rotated around the z-axis. After the calculation and comparison, the performance of the motor is best when the second layer rotates 18° and the third layer rotates 36° . According to the major electromagnetic characteristics of basic and optimized models, it verifies the effectiveness of the optimized structure.

REFERENCES

- [1] Fukui, S., et al., Numerical Study of Optimization Design of High Temperature Superconducting Field Winding in 20 MW Synchronous

- Motor for Ship Propulsion. IEEE Transactions on Applied Superconductivity, 2012. 22(3): p. 5200504-5200504.
- [2] Eckels, P.W. and G. Snitchler, 5 MW High Temperature Superconductor Ship Propulsion Motor Design and Test Results. Naval Engineers Journal, 2005. 117(4): p. 31-36.
- [3] Baik, S.K., et al., Design Considerations for 1 MW Class HTS Synchronous Motor. IEEE Transactions on Applied Superconductivity, 2005. 15(2): p. 2202-2205.
- [4] The Design of a Lightweight HTS Synchronous Generator Cooled by Subcooled Liquid Nitrogen
- [5] Kajikawa, Kazuhiro, et al. "Development of Stator Windings for Fully Superconducting Motor With Wires." IEEE Transactions on Applied Superconductivity 23.3(2013):5201604-5201604.
- [6] Pina, J.M., M.V. Neves and A.L. Rodrigues, Case study in the design of HTS machines: an all superconducting linear synchronous motor. 2007. p. 185-190.
- [7] Masson, P.J., et al., Development of a 3D Sizing Model for All-Superconducting Machines for Turbo-Electric Aircraft Propulsion. IEEE Transactions on Applied Superconductivity, 2013. 23(3): p. 3600805-3600805.
- [8] P., T., et al., 150-kW experimental superconducting permanent-magnet motor. Geophysics, 1999. 9(2): p. 1205-1208.
- [9] Tamura, K., et al., Study on the Optimum Arrangement of the Field Winding for a 20-kW Fully Superconducting Motor. IEEE Transactions on Applied Superconductivity, 2016. 26(4): p. 1-5. [10] Kashani, M., M. Hosseina and A. Darabi, Design of Synchronous Motor with High-temperature Superconductive Field Windings for Marine Propulsion Applications. ELECTRIC POWER COMPONENTS AND SYSTEMS, 2013. 41(4): p. 413-426.
- [11] Huang, Zhen, et al. "Trial Test of a Bulk-Type Fully HTS Synchronous Motor." IEEE Transactions on Applied Superconductivity 24.3(2014):1-5.
- [12] Koshiba, Y., et al. "Critical Current and Electric Loss Under Magnetic Field at 30 K on Bi-2223 Superconducting Coil for Ship Propulsion Motor." IEEE Transactions on Applied Superconductivity 21.3(2011):1127-1130.
- [13] Boldea, Ion. The induction machines design handbook. CRC press, 2009.